PXR Ablation Alleviates Diet-Induced and Genetic Obesity and Insulin Resistance in Mice

Jinhan He,[1,2] Jie Gao,[1] Meishu Xu,[1] Songrong Ren,[1] Maja Stefanovic-Racic,[3] Robert Martin O'Doherty,[3] and Wen Xie[1,4]

The pregnane X receptor (PXR), along with its sister receptor constitutive androstane receptor (CAR), was initially characterized as a xenobiotic receptor that regulates drug metabolism. In this study, we have uncovered an unexpected endobiotic role of PXR in obesity and type 2 diabetes. PXR ablation inhibited high-fat diet (HFD)–induced obesity, hepatic steatosis, and insulin resistance, which were accounted for by increased oxygen consumption, increased mitochondrial β-oxidation, inhibition of hepatic lipogenesis and inflammation, and sensitization of insulin signaling. In an independent model, introducing the $PXR^{-/-}$ allele into the *ob/ob* background also improved body composition and relieved the diabetic phenotype. The *ob/ob* mice deficient of PXR showed increased oxygen consumption and energy expenditure, as well as inhibition of gluconeogenesis and increased rate of glucose disposal during euglycemic clamp. Mechanistically, the metabolic benefits of PXR ablation were associated with the inhibition of c-Jun NH_2-terminal kinase activation and downregulation of lipin-1, a novel PXR target gene. The metabolic benefit of PXR ablation was opposite to the reported prodiabetic effect of CAR ablation. Our results may help to establish PXR as a novel therapeutic target, and PXR antagonists may be used for the prevention and treatment of obesity and type 2 diabetes. ***Diabetes*** **62:1876–1887, 2013**

The pregnane X receptor (PXR), predominantly expressed in the liver and intestine, is a nuclear receptor that responds to a wide variety of drugs, other xenobiotics, and endogenous compounds (1,2). PXR was initially defined as a xenobiotic receptor that regulates the expression of drug-metabolizing enzymes and transporters. Subsequent studies showed that PXR has much more diverse functions, ranging from drug metabolism to bile acid and bilirubin detoxification, homeostasis of glucocorticoids, mineralocorticoids, and androgens, vitamin metabolism and bone mineral homeostasis, retinoic acid metabolism, and anti-inflammation (3,4). However, whether PXR plays a role in the pathogenesis of obesity and insulin-resistant type 2 diabetes is not known.

From the [1]Center for Pharmacogenetics and Department of Pharmaceutical Sciences, University of Pittsburgh, Pittsburgh, Pennsylvania; the [2]Department of Pharmacy, West China Hospital, Sichuan University, Chengdu, Sichuan, China; the [3]Division of Endocrinology and Metabolism, Department of Medicine, University of Pittsburgh, Pittsburgh, Pennsylvania; and the [4]Department of Pharmacology and Chemical Biology, University of Pittsburgh, Pittsburgh, Pennsylvania.

Corresponding author: Wen Xie, wex6@pitt.edu.

Received 1 August 2012 and accepted 15 January 2013.

DOI: 10.2337/db12-1039

This article contains Supplementary Data online at http://diabetes.diabetesjournals.org/lookup/suppl/doi:10.2337/db12-1039/-/DC1.

It has been well recognized that certain classes of drugs can cause clinically significant elevations in blood glucose (5,6). Interestingly, many known PXR-activating drugs, such as rifampicin (1), statins (7), phenytoin (8), and cyclophosphamide (9), can induce hyperglycemia in patients. An early phase of hyperglycemia, associated with increased rates of insulin secretion, was observed among patients taking rifampicin (10). Statin therapies are associated with an increased risk for developing diabetes (11). Phenytoin has been shown to induce hyperglycemia and hyperinsulinemia (12–15). Cyclophosphamide has been reported to cause elevated blood glucose levels during chemotherapy (16,17). These reports suggest that PXR might be involved in the drug-induced metabolic disorders.

Recent studies have indeed linked PXR to lipid and glucose metabolism. Activation of PXR induces hepatic steatosis by increasing fatty acid uptake and inhibiting fatty acid β-oxidation (18,19). PXR binds directly to the forkhead factor A2 and represses its activation of Cpt-1α, a rate-limiting enzyme of mitochondrial fatty acid β-oxidation (18). PXR also inhibits the expression of the gluconeogenic enzymes PEPCK and G6Pase by cross-talk with the cAMP-responsive element binding protein and forkhead box protein O1, two positive transcriptional regulators of gluconeogenesis (20,21). In addition, PXR competes with HNF-4α for the binding to PGC-1α, suggesting yet another mechanism by which PXR might suppress hepatic gluconeogenesis (22). These results together suggest that PXR has a complex role in energy homeostasis (23). However, most of these reports were derived from in vitro studies or they have been largely focused on the fatty liver phenotype (19,24). It was recently reported that a chronic treatment of AKR/J mice with a high dose of pregnenolone-16α-carbonitrile (PCN), a mouse PXR agonist, prevented high-fat diet (HFD)–induced obesity and insulin resistance (25), suggesting a potential role of PXR in energy metabolism in vivo.

In this study, we uncovered a previously unknown function of PXR in obesity and insulin resistance. PXR ablation protected mice from dietary and genetically induced obesity and insulin resistance. In contrast, transgenic activation of PXR in *ob/ob* mice exacerbated insulin resistance. Our results may establish this "xenobiotic receptor" as a novel therapeutic target for the prevention and treatment of obesity and type 2 diabetes.

RESEARCH DESIGN AND METHODS

Animals, diet treatment, body composition analysis, histology, and drug treatment. $PXR^{-/-}$ and *Alb-VP-PXR* mice were previously described (26), and they have been backcrossed to the C57BL/6J background for at least eight generations. *Obp* mice (*ob/ob* mice deficient of PXR) and $ob/ob^{VP\text{-}PXR}$ mice (*ob/ob* mice expressing the *Alb-VP-PXR* transgene) were generated by breeding the $PXR^{-/-}$ allele and *Alb-VP-PXR* transgene into the *ob/ob* background, respectively. In the HFD model, 6-week-old mice received an HFD (S3282) from Bio-Serv (Frenchtown, NJ) for 12 weeks (27,28). The food intake was

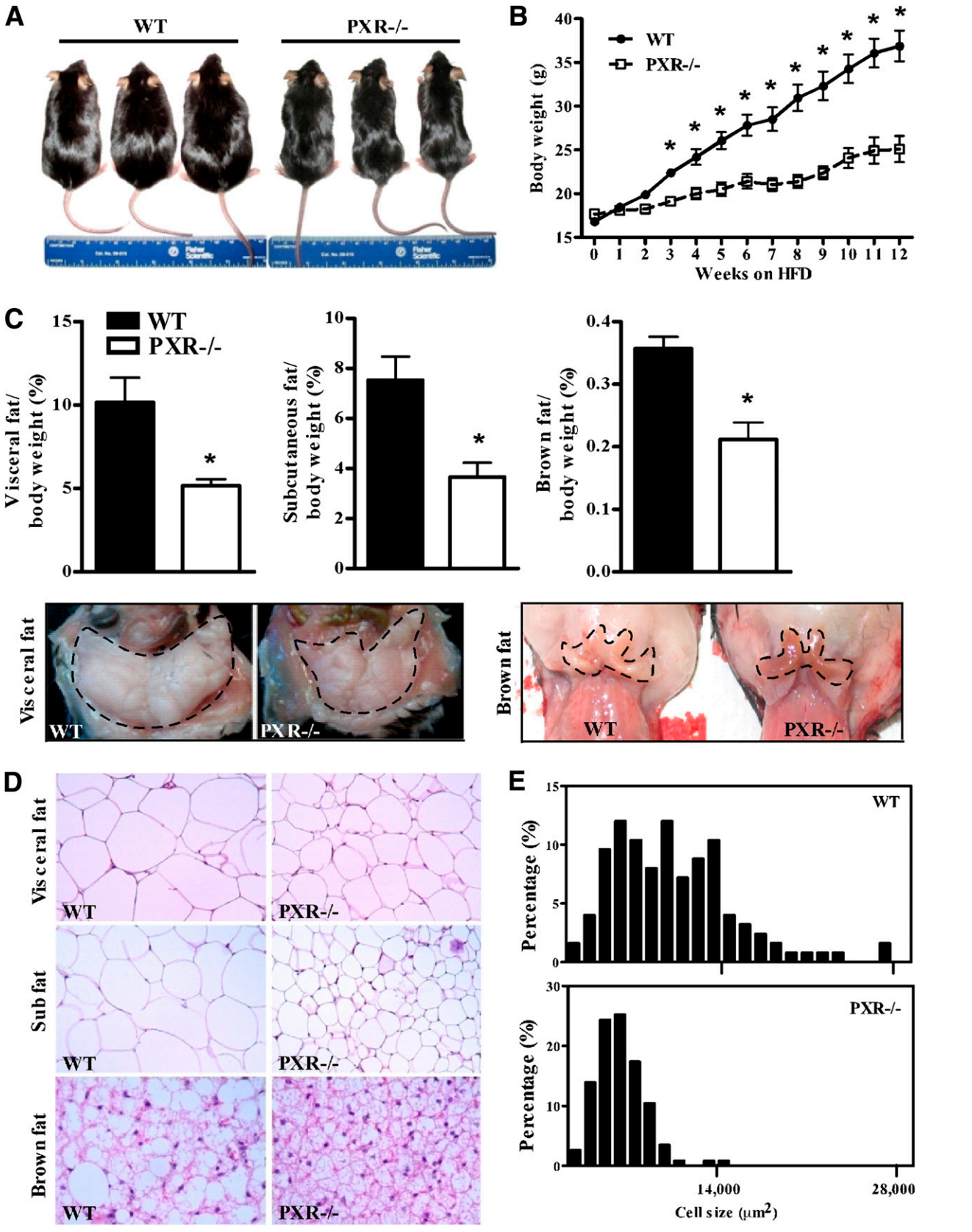

FIG. 1. PXR ablation inhibited HFD-induced obesity. WT and $PXR^{-/-}$ mice were fed with HFD for 12 weeks. *A*: Appearance of WT and $PXR^{-/-}$ mice at the end of HFD feeding. *B*: Growth curve of WT and $PXR^{-/-}$ mice. $n = 5$ for each group. *C*: The fat weight/body weight ratio in three different fat depots (*top*) and representative appearance of visceral and brown fat tissues (*bottom*). *D* and *E*: Histological analysis of three fat depots (*D*) and distribution of adipocyte size of the visceral fat (*E*). *$P < 0.05$, $PXR^{-/-}$ vs. WT. (A high-quality color representation of this figure is available in the online issue.)

measured for 7 days after 12 weeks of HFD feeding, and the data were normalized to lean content of body weight. *Ob/ob*, *obp*, and *ob/ob*$^{VP\text{-}PXR}$ were maintained in control chow diet. Body composition was analyzed in live animals using EchoMRI-100TM from Echo Medical Systems (Houston, TX). To quantify fat mass, visceral and subcutaneous fat was carefully dissected after mice were killed. The fat mass was weighed and normalized to the body weight. For histological analysis, tissues were fixed in 4% formaldehyde, embedded in paraffin, sectioned at 5 μm, and stained with hematoxylin and eosin (H&E). To quantify adipocyte sizes, digital images of H&E staining sections were converted into binary format with Adobe Photoshop 7.0, and the adipocyte surface areas were quantified using the Image Processing Tool Kit from Reindeer Games (Gainesville, FL) as previously described (29). Frozen sections (8 μm) were used for Oil-red O staining. When necessary, mice received daily intraperitoneal injections of PCN (20 mg/kg) for 3 days, or ketoconazole (20 mg/kg) for 2 weeks, before tissue harvesting. For tunicamycin treatment, mice received a single intraperitoneal injection of tunicamycin (1 mg/kg) 6 h before tissue harvesting. The use of mice in this study has complied with relevant federal guidelines and institutional policies.

Measurement of serum parameters. Blood samples were collected from fed or fasted mice. Serum levels of total triglycerides and cholesterol (Stanbio Laboratory, Boerne, TX), free fatty acids (Biovision, Mountain View, CA), and insulin and leptin (Crystal Chem, Downers Grove, IL) were measured by using commercial assay kits.

Indirect calorimetry, glucose tolerance test, insulin tolerance test, and euglycemic-hyperinsulinemic clamp. Indirect calorimetry was performed using the Oxymax Indirect Calorimetry System/metabolic cages from Columbus Instruments (Columbus, OH) as we have previously described (28). The glucose tolerance tests (GTTs), insulin tolerance tests (ITTs) (28), and clamp experiments (27) were performed as we have previously described.

Western blot analysis. To measure insulin signaling in vivo, mice received a bolus injection of 1 unit/kg insulin or saline through a portal vein. The liver tissues were harvested 5 min after the injection. The primary antibodies used include those against p-AKT (serine 473), AKT, p-PERK (Thr980), PERK, phosphorylated c-Jun NH_2-terminal kinase (p-JNK), and JNK from Cell Signaling (Danvers, MA); PXR from Santa Cruz (Santa Cruz, CA); and insulin receptor substrate-1 (IRS-1) (pSer307) from Millipore (Billerica, MA). For Western blot on primary mouse hepatocytes, cells were treated with vehicle or tunicamycin (1 μg/mL) and/or insulin (100 nmol/L) for 2 h.

Glucose production assay. Mouse primary hepatocytes were plated onto collagen-coated six-well plates at a density of 2×10^5 cells/well. After cells attached for 2 h, the medium was changed to hepatocyte maintain medium in the presence or absence of 10 μmol/L ketoconazole for overnight. The cells were then washed three times with PBS before being incubated for 2 h in the presence or absence of 10 μmol/L forskolin. Medium was collected and glucose was assayed using a hexokinase-based glucose assay kit from Sigma-Aldrich. The glucose levels were normalized to protein concentrations in the cell lysates of the same plates of cells.

Electrophoretic mobility shift assay and transient transfection and luciferase reporter gene assay. Electrophoretic mobility shift assay was performed using ^{32}P-labeled oligonucleotides and receptor proteins prepared by the TNT method (19). The mouse lipin-1 gene promoter (2-kb) luciferase reporter plasmid was a gift from Dr. Brian N. Finck (Washington University School of Medicine, St. Louis, MO). HepG2 cells were transfected with the reporter construct and PXR expression vector in 48-well plates as previously described (19). When necessary, cells were treated with PCN (10 μmol/L) for 24 h before luciferase assay. The transfection efficiency was normalized against the β-galactosidase activities from a cotransfected CMX β-galactosidase vector.

VLDL secretion assay. VLDL secretion rate in vivo was measured as we have described previously (28).

Measurement of tissue mitochondrial fatty acid oxidation. Liver and skeletal muscle mitochondrial fatty acid oxidation was measured as described previously (28). In brief, fresh tissues were excised and placed in ice-cold modified Chappell-Perry buffer. Tissue homogenates were prepared, and mitochondria were isolated using differential centrifugation. Oxidation assays were performed using 0.2 mmol/L [^{14}C]-oleate in the absence or presence of 2 mmol/L sodium pyruvate. Reactions were terminated by adding 100 μL 70% perchlori acid, and [^{14}C]-CO_2 was trapped in 200 μL of 1 N NaOH. [^{14}C]CO_2 and ^{14}C-labeled acid-soluble metabolites were assessed by liquid scintillation counting.

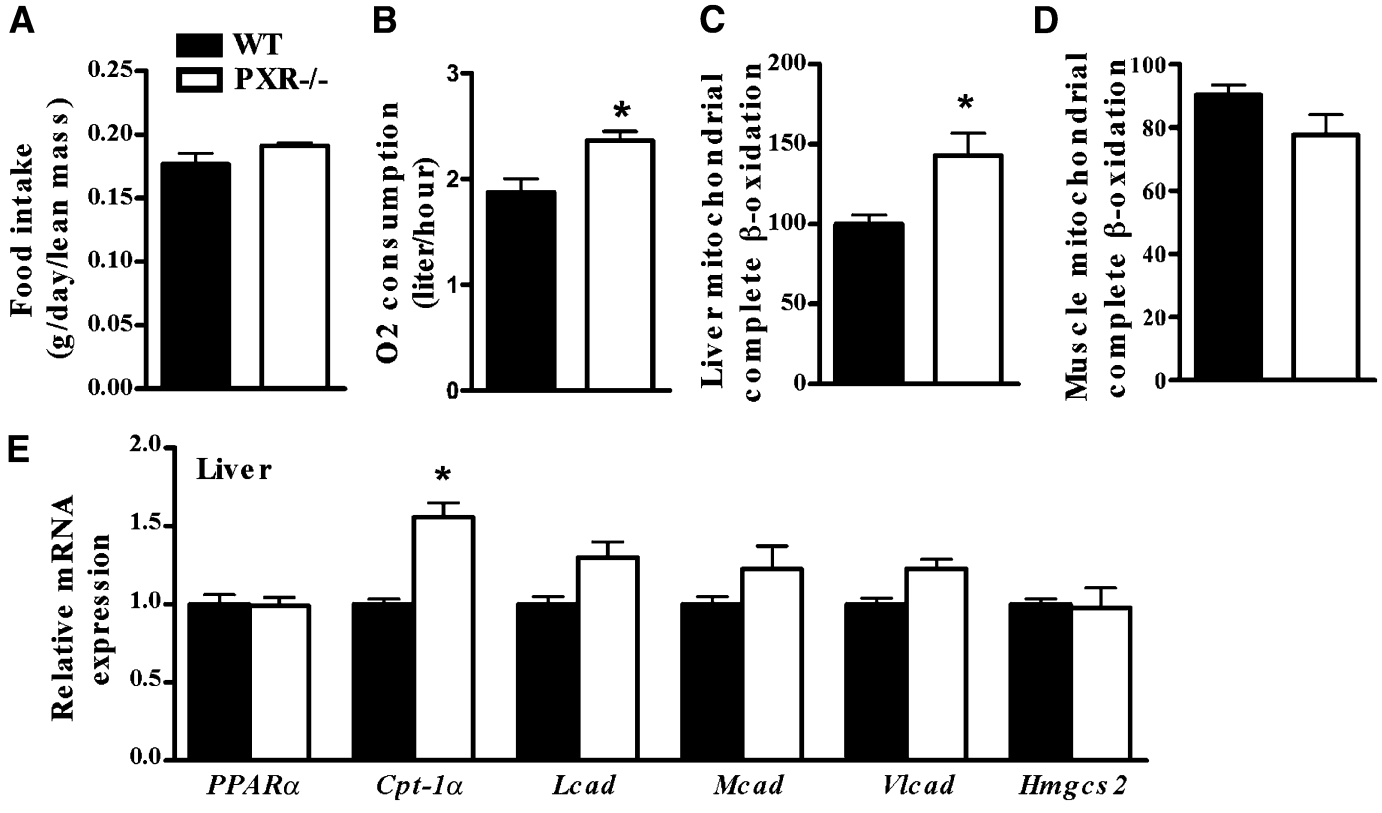

FIG. 2. PXR ablation increased oxygen consumption and liver mitochondrial β-oxidation. WT and *PXR*$^{-/-}$ mice were the same as described in Fig. 1. Food intake (*A*) and oxygen consumption (*B*). Liver (*C*) and gastrocnemius muscle (*D*) fatty acid β-oxidation. Fresh tissues were homogenized and mitochondria were isolated. Oxidation was measured by [^{14}C]-CO_2 production from [^{14}C]-oleate. *E*: Hepatic mRNA expression of β-oxidation genes as measured by real-time PCR. *n* = 5 for each group. **P* < 0.05, PXR$^{-/-}$ vs. WT.

Gene expression analysis. For real-time PCR analysis, reverse transcription was performed with random hexamer primers and Superscript RT III enzyme from Invitrogen. SYBR Green–based real-time PCR was performed with the ABI 7300 real-time PCR system (28). Data were normalized against the control cyclophilin. Sequences of the real-time PCR probes are listed in Supplementary Table 1.

RESULTS

PXR ablation inhibited HFD-induced obesity. To evaluate the function of PXR in energy metabolism, age-matched wild-type (WT) and $PXR^{-/-}$ mice were fed with normal chow diet or HFD for 12 weeks. Under the chow diet, $PXR^{-/-}$ and WT mice were not different in their body weights (data not shown) and total fat or lean content (Supplementary Fig. 1*A*). However, after 12 weeks of HFD feeding, $PXR^{-/-}$ mice were visibly smaller (Fig. 1*A*) and ~29% lower in body weight than their WT counterparts (Fig. 1*B*). Necropsy revealed that $PXR^{-/-}$ mice had a significantly decreased mass of visceral fat, subcutaneous fat, and brown adipose tissue (Fig. 1*C*). The total fat mass and lean mass were decreased and increased in HFD-fed $PXR^{-/-}$ mice, respectively (Supplementary Fig. 1*B*). H&E staining showed decreased adipocyte sizes in all three fat depots of $PXR^{-/-}$ mice (Fig. 1*D*). The decreased adipocyte size in the visceral fat of $PXR^{-/-}$ mice was supported by cell size quantification (Fig. 1*E*).

PXR ablation increased oxygen consumption and liver mitochondrial β-oxidation. To understand the mechanism by which PXR ablation inhibited HFD-induced obesity,

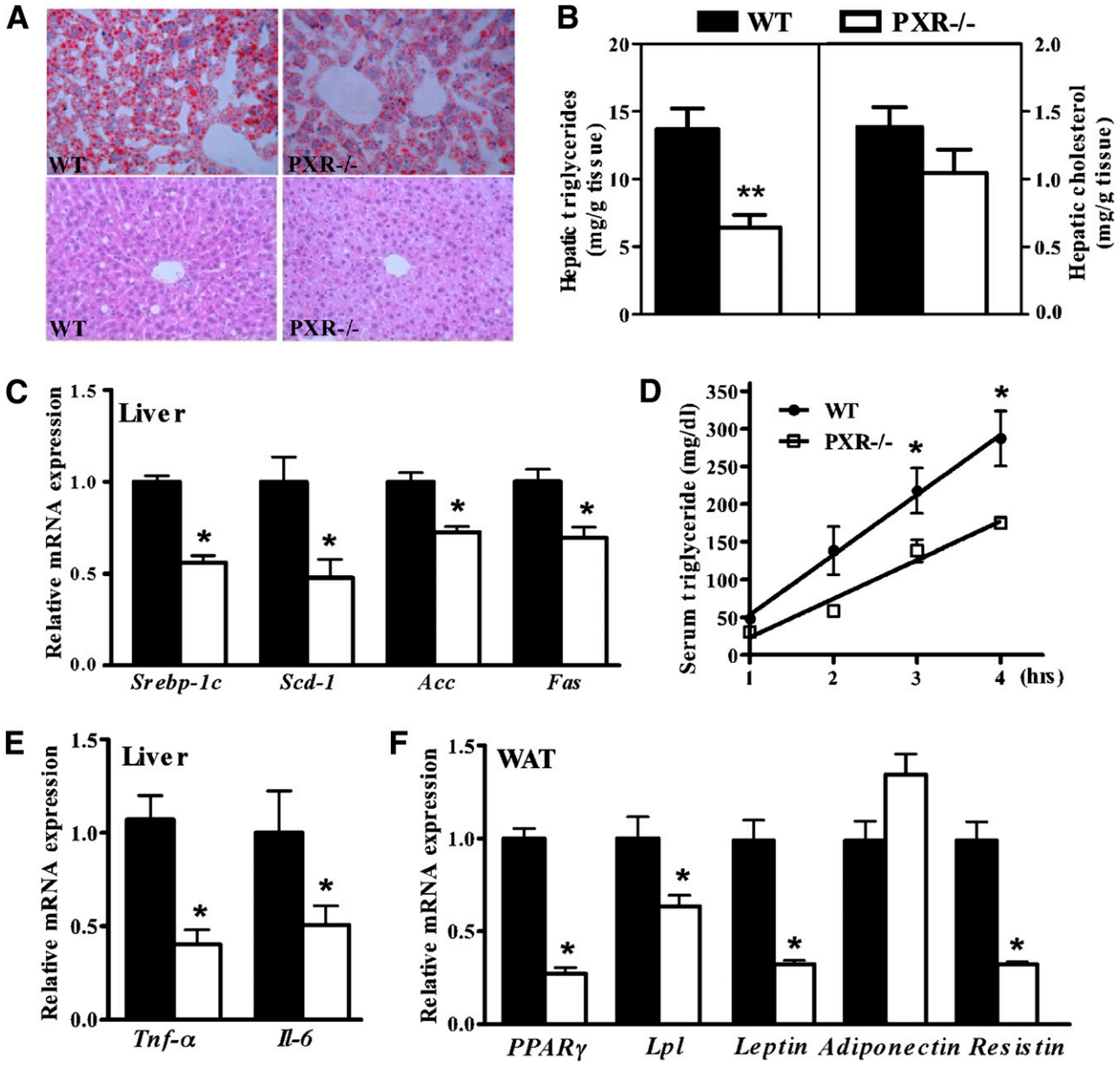

FIG. 3. PXR ablation inhibited HFD-induced hepatic steatosis and inflammation. WT and $PXR^{-/-}$ mice were the same as described in Fig. 1. *A*: Oil-red O (*top*) and H&E staining (*bottom*) of the liver sections. *B*: Hepatic triglyceride and cholesterol contents. *C*: Hepatic mRNA expression of lipogenic genes as measured by real-time PCR. *D*: VLDL-triglyceride secretion rate. Mice were fasted for 4 h before receiving an intravenous injection of tyloxapol (500 mg/kg body weight). Blood was sampled and measured for serum concentrations of triglycerides. Liver (*E*) and WAT (*F*) mRNA expression of indicated genes as measured by real-time PCR. $n = 5$ for each group. *$P < 0.05$, $PXR^{-/-}$ vs. WT; **$P < 0.01$ $PXR^{-/-}$ vs. WT mice. (A high-quality color representation of this figure is available in the online issue.)

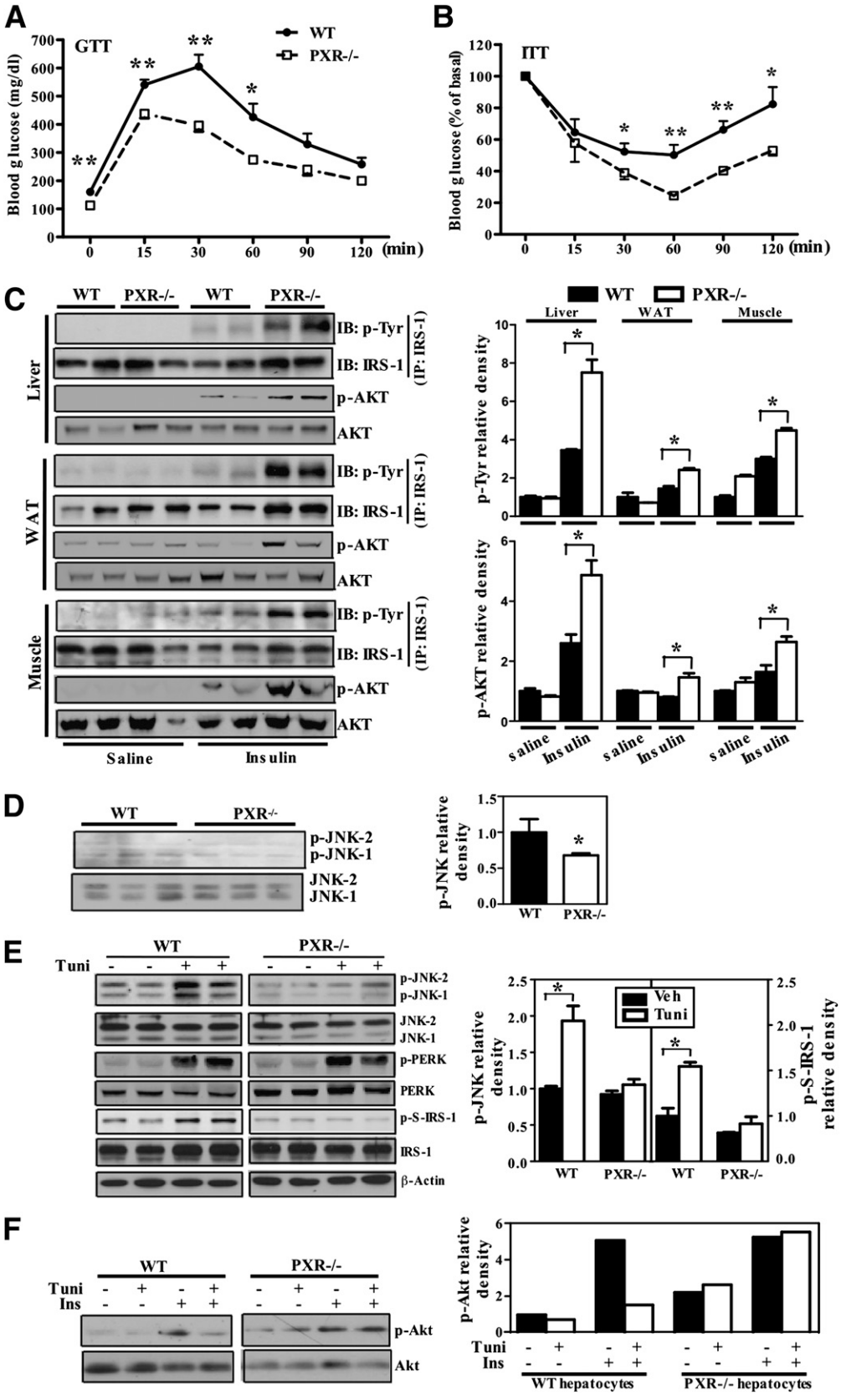

FIG. 4. PXR ablation improved insulin sensitivity and inhibited JNK activation. *A* and *B*: GTT and ITT in WT and $PXR^{-/-}$ mice fed with HFD for 12 weeks. *C*: After 12 weeks of HFD feeding, mice received a bolus injection of insulin (1 units/kg) through the portal vein. Five minutes later, tissues were harvested for Western blot analysis. *Left*: Tissue extracts were immunoprecipitated for IRS-1 and immunoblotted (IB) for phosphorylated and total IRS-1. The immunoblots for phosphorylated and total AKT were performed without immunoprecipitation. *Right*: Quantification of the Western blot results. $n = 6$ for each group. *D*: Liver JNK phosphorylation and quantification in mice described in *A*. *E*: Western blot measurement of liver JNK phosphorylation, IRS-1 serine phosphorylation, and PERK phosphorylation, as well as their quantifications in WT and $PXR^{-/-}$ mice 6 h

we measured food uptake and energy expenditure in these two genotypes. The $PXR^{-/-}$ and WT mice consumed a comparable amount of food (Fig. 2*A*). However the energy expenditure, as indicated by oxygen consumption, was significantly higher in $PXR^{-/-}$ mice (Fig. 2*B*). The higher oxygen consumption in $PXR^{-/-}$ mice was accompanied by increased complete mitochondrial fatty acid β-oxidation in the liver (Fig. 2*C*). In contrast, the β-oxidation was not significantly different between $PXR^{-/-}$ and WT mice in the gastrocnemius muscle (Fig. 2*D*), consistent with the lack of PXR expression in the skeletal muscle (1,2). The higher β-oxidation in $PXR^{-/-}$ mice was supported by the increased β-oxidation gene expression, among which the induction of CPT-1α was the most prominent (Fig. 2*E*).

PXR ablation inhibited HFD-induced hepatic steatosis and inflammation. The HFD model is known to be associated with hepatic steatosis. Oil-red O staining showed a decreased lipid staining in the liver of $PXR^{-/-}$ mice (Fig. 3*A*). Lipid analysis showed that the hepatic triglyceride level, but not the cholesterol level, was significantly decreased in $PXR^{-/-}$ mice (Fig. 3*B*). Consistent with the inhibition of steatosis, the expression of hepatic lipogenic genes, including *Srebp-1c*, *Scd-1*, *Acc*, and *Fas*, was suppressed in $PXR^{-/-}$ mice (Fig. 3*C*). $PXR^{-/-}$ mice also showed a decreased VLDL-triglyceride secretion (Fig. 3*D*), suggesting that the inhibition of steatosis in these mice was not due to an increased triglyceride secretion. The inhibition of hepatic steatosis in $PXR^{-/-}$ mice was associated with a decreased expression of inflammatory cytokine genes *Tnf-α* and *Il-6* in the liver (Fig. 3*E*). When the white adipose tissue (WAT) was examined, we found the expression of *PPARγ* and lipoprotein lipase (*Lpl*), two adipogenic genes, was decreased in $PXR^{-/-}$ mice (Fig. 3*F*). $PXR^{-/-}$ mice also showed lower leptin and resistin gene expression in WAT (Fig. 3*F*), which suggested an improved insulin sensitivity.

PXR ablation improved insulin sensitivity and inhibited c-Jun NH_2-terminal kinase activation. A sustained HFD feeding will lead to insulin resistance and type 2 diabetes. The improved metabolic function of $PXR^{-/-}$ mice led to our hypothesis that $PXR^{-/-}$ mice may have improved glucose metabolism and insulin sensitivity. $PXR^{-/-}$ and WT mice maintained on chow diet showed similar glucose (Supplementary Fig. 1*C*) and insulin (Supplementary Fig. 1*D*) tolerance. Upon HFD feeding, $PXR^{-/-}$ mice showed significantly improved glucose (Fig. 4*A*) and insulin (Fig. 4*B*) tolerance. In understanding the mechanism by which PXR ablation improved insulin sensitivity, we assessed insulin signaling sensitivity in the liver, WAT, and skeletal muscle. In this experiment, mice fed with HFD for 12 weeks were fasted overnight before being administered saline or insulin through the portal vein. We found that the insulin-induced tyrosine phosphorylation of both the IRS-1 and AKT was enhanced in all three tissues (Fig. 4*C*), suggesting a systemically improved insulin sensitivity. Serum chemistry also supported the improved insulin sensitivity in $PXR^{-/-}$ mice, including their decreased fasting and fed serum levels of glucose, insulin, cholesterol, and leptin (Table 1). Interestingly, the serum level of triglycerides was not significantly affected in $PXR^{-/-}$ mice.

Activation of c-Jun NH_2-terminal kinase (JNK) and subsequent serine phosphorylation of IRS-1 plays a central role in obesity-induced insulin resistance (30). To understand the mechanism by which PXR ablation improved insulin sensitivity, we evaluated whether JNK activation was inhibited in $PXR^{-/-}$ mice. Indeed, JNK phosphorylation was reduced in the liver of HFD-fed $PXR^{-/-}$ mice (Fig. 4*D*). Cellular stress has been known to induce JNK activation (31), and tunicamycin is a prototypical cellular stressor chemical. We found that the tunicamycin-induced JNK phosphorylation observed in the liver of WT mice was inhibited in $PXR^{-/-}$ mice (Fig. 4*E*). In contrast, the tunicamycin-induced serine phosphorylation of IRS-1 was abolished in $PXR^{-/-}$ mice (Fig. 4*E*). Interestingly, the tunicamycin-induced phosphorylation of PERK, a typical marker for endoplasmic reticulum stress, was found to be intact in $PXR^{-/-}$ mice (Fig. 4*E*). In WT hepatocytes, the insulin-responsive phosphorylation of AKT was inhibited by the cotreatment of tunicamycin, but this inhibition was abolished in $PXR^{-/-}$ hepatocytes (Fig. 4*F*), also suggesting an improved insulin sensitivity.

PXR ablation improved metabolic function and insulin sensitivity in *ob/ob* mice. We bred the $PXR^{-/-}$ allele into the *ob/ob* background to determine whether the metabolic benefit of PXR ablation can be extended to this genetic model of obesity and type 2 diabetes. The PXR-deficient *ob/ob* mice, which we termed "*obp*" mice, were maintained on chow diet. At 16 weeks of age, although the *obp* mice showed a similar body weight as their *ob/ob* counterparts, MRI analysis showed that *obp* mice had significantly decreased fat mass and increased lean mass (Fig. 5*A*). Necropsy also showed a marked reduction in the weight of WAT depots in *obp* mice (Fig. 5*B*). The difference in adiposity was not attributable to a reduction in food consumption, because food intakes were indistinguishable between these two genotypes (Fig. 5*C*). Instead, we found that both the oxygen consumption (Fig. 5*D*) and dark-phase energy expenditure (Fig. 5*E*) were significantly increased in *obp* mice. Histological analysis showed decreased hepatic steatosis and adipocyte size in *obp* mice (Fig. 5*F*). The inhibition of steatosis in *obp* mice was confirmed by their decreased levels of hepatic triglycerides, but not cholesterol (Fig. 5*G*).

When the insulin sensitivity of the *obp* mice was examined and compared with that of the *ob/ob* mice, we found that *obp* mice showed improved performance in GTTs (Fig. 6*A*) and ITTs (Fig. 6*B*). In agreement with the GTT and ITT results, *obp* mice showed lower fasting blood glucose (Fig. 6*C*) and insulin (Fig. 6*D*) levels. The mRNA expression of hepatic gluconeogenic genes *Pepck* and *G6Pase* was lower in *obp* mice (Fig. 6*E*). To evaluate the effect of PXR ablation on peripheral and hepatic insulin action, we performed the hyperinsulinemic-euglycemic clamp on *ob/ob* and *obp* mice. The glucose infusion rate necessary to maintain euglycemia in *obp* mice was ~50% higher than in *ob/ob* mice (Fig. 6*F*), indicating enhanced insulin-stimulated glucose uptake and metabolism in *obp* mice. The suppression of hepatic glucose production by insulin during the clamp stage was also greatly enhanced in *obp* mice (Fig. 6*G*). Blood glucose and insulin levels in the basal and clamp state are shown in Fig. 6*H* and *I*, respectively.

after receiving a single intraperitoneal injection of tunicamycin (1 mg/kg). In the quantification, the left and right panels are for JNK phosphorylation and IRS-1 serine phosphorylation, respectively. *F*: Primary hepatocytes from WT and $PXR^{-/-}$ mice were treated with vehicle or tunicamycin (1 μg/mL) and/or insulin (100 nmol/L) for 2 h before Western blot analysis for the detection of phosphorylated and total AKT. Quantifications are shown in the right panel. *$P < 0.05$; **$P < 0.001$, $PXR^{-/-}$ vs. WT, or the comparisons are labeled.

TABLE 1
Serum parameters in WT and $PXR^{-/-}$ mice fed with HFD for 12 weeks

	Fasting		Fed	
	WT	$PXR^{-/-}$	WT	$PXR^{-/-}$
Glucose (mg/dL)	160.51 ± 5.88	98.83 ± 6.32**	190.51 ± 9.17	133.2 ± 7.08**
Insulin (ng/mL)	0.54 ± 0.05	0.19 ± 0.04**	2.21 ± 0.45	0.52 ± 0.04**
Triglycerides (mg/dL)	64.09 ± 14.54	46.79 ± 6.14	69.29 ± 5.06	60.41 ± 3.95
Cholesterol (mg/dL)	133.81 ± 8.63	108.4 ± 7.24*	217.21 ± 3.71	157.31 ± 5.13**
Leptin (ng/mL)	26.29 ± 2.27	12.16 ± 2.28**	30.96 ± 0.78	17.51 ± 3.74**

*$P < 0.05$. **$P < 0.01$, $PXR^{-/-}$ vs. WT.

Transgenic activation of PXR exacerbated the diabetic phenotype of *ob/ob* mice. The improved metabolic function associated with PXR ablation prompted us to determine whether activation of PXR confers heightened sensitivity to metabolic abnormalities. For this purpose, we bred the liver-specific *Alb-VP-PXR* transgene (26) into the *ob/ob* background to generate the $ob/ob^{VP\text{-}PXR}$ mice. The *Alb-VP-PXR* transgene directs the expression of the constitutively activated PXR (VP-PXR) under the control of the liver-specific albumin (*Alb*) gene promoter (26). Indeed, the $ob/ob^{VP\text{-}PXR}$ mice showed worsened hypertriglyceridemia with their serum triglyceride level ~50% higher than the *ob/ob* mice (Fig. 7*A*). The $ob/ob^{VP\text{-}PXR}$ mice also showed an increased hepatic triglyceride level (Fig. 7*B*). The expression of multiple lipogenic genes (Fig. 7*C*) and β-oxidation genes (Fig. 7*D*) was elevated and reduced in $ob/ob^{VP\text{-}PXR}$ mice, respectively. The decreased β-oxidation gene expression was accompanied by decreased mitochondrial fatty acid β-oxidation (Fig. 7*E*). Finally, compared with the *ob/ob* mice, the $ob/ob^{VP\text{-}PXR}$ mice showed worsened glucose tolerance (Fig. 7*F*) and insulin intolerance (Fig. 7*G*).

Interestingly, despite having worsened diabetic phenotypes, the $ob/ob^{VP\text{-}PXR}$ mice had a modest, but significant, decrease in body weight compared with *ob/ob* mice (Supplementary Fig. 2*A*), suggesting that that a decreased body is not always translated into a better metabolic function. The fat cell size was not different between these two genotypes (Supplementary Fig. 2*B*).

Treatment with the PXR antagonist ketoconazole modestly improved the metabolic function of HFD-fed mice. To determine whether the use of a PXR antagonist is a therapeutically viable approach to improve metabolic function, C57BL/6J mice were fed with HFD for 10 weeks before being given daily intraperitoneal injections of ketoconazole (20 mg/kg) or vehicle for 2 weeks while the mice remained on HFD. As shown in Supplementary Fig. 3, this regimen of ketoconazole modestly improved the GTT performance at late time points (Supplementary Fig. 3*A*) but did not have a significant effect on the ITT performance (Supplementary Fig. 3*B*). Gene expression analyses showed that treatment of ketoconazole significantly inhibited the expression of PEPCK (Supplementary Fig. 3*C*), but had little effect on the expression of G6Pase (Supplementary Fig. 3*C*), lipogenic genes (Supplementary Fig. 3*D*), or β-oxidation gene expression (Supplementary Fig. 3*E*). Ketoconazole treatment also decreased the basal expression of Cyp3a11 and did not cause a body weight difference between the vehicle and ketoconazole groups (data not shown), suggesting that this regimen of ketoconazole was functional as a PXR antagonist and was not toxic to the mice.

Lipin-1 is a PXR target gene. Lipin-1 is a member of the mammalian Mg^{2+}-dependent phosphatidic acid phosphatase. Hepatic expression of lipin-1 has been shown to increase triglyceride synthesis and VLDL secretion (32). Hepatic overexpression of lipin-1 has also been reported to increase JNK phosphorylation and perturb insulin signaling (33). In contrast, knockdown of lipin-1 ameliorates hyperglycemia and insulin resistance in obese mice (33). Our Affymetrix microarray analysis showed that the expression of lipin-1 was decreased in the liver of HFD-fed $PXR^{-/-}$ mice and chow-fed *obp* mice (data not shown), and the microarray results were confirmed by real-time PCR analysis (Supplementary Fig. 4*A*). In the gain-of-function models, the hepatic expression of lipin-1 was increased when PXR was pharmacologically activated by PCN, or genetically activated in the $ob/ob^{VP\text{-}PXR}$ mice (Supplementary Fig. 4*B*). To determine whether lipin-1 is a PXR target gene, we inspected the mouse lipin-1 gene promoter and found a direct repeat spaced by three nucleotides (DR3) type putative PXR binding site (Supplementary Fig. 4*C*). Electrophoretic mobility shift assay showed that the PXR-retinoic X receptor (RXR) heterodimers can bind to this DR3, and this binding can be efficiently competed by excess unlabeled DR3, but not by the mutant DR3 (Supplementary Fig. 4*C*). Furthermore, a luciferase reporter gene containing the 2-kb mouse lipin-1 gene promoter was activated by PXR in the presence of the PXR agonist PCN, and mutation of the DR3 abolished the PXR-dependent transactivation (Supplementary Fig. 4*D*). These results suggested lipin-1 as a PXR target gene, providing a plausible mechanism by which activation of PXR may worsen the metabolic functions.

DISCUSSION

In this study, we reported that $PXR^{-/-}$ mice were markedly alleviated from diet and genetically induced obesity and insulin resistance. The metabolic benefits of PXR deficiency may have resulted from the combined effect of elevation of oxygen consumption and β-oxidation, and inhibition of lipogenesis and gluconeogenesis. In contrast, transgenic activation of PXR in *ob/ob* mice caused hyperlipidemia and exacerbated insulin resistance. Mechanistically, PXR deficiency confers resistance to cellular stress–induced JNK activation and improves insulin signaling. The regulation of lipin-1, whose gene product is known to increase triglyceride synthesis and perturb insulin signaling, by PXR may have also contributed to the metabolic consequences of PXR ablation or activation. However, future uses of lipin-1 knockout or transgenic mice are necessary to determine whether the expression and/or regulation of lipin-1 are important for the metabolic effect of PXR. It was noted that the mRNA and protein levels of PXR were not changed in HFD-fed or *ob/ob* mice (data not shown). Although the effect of PXR genotypes on the

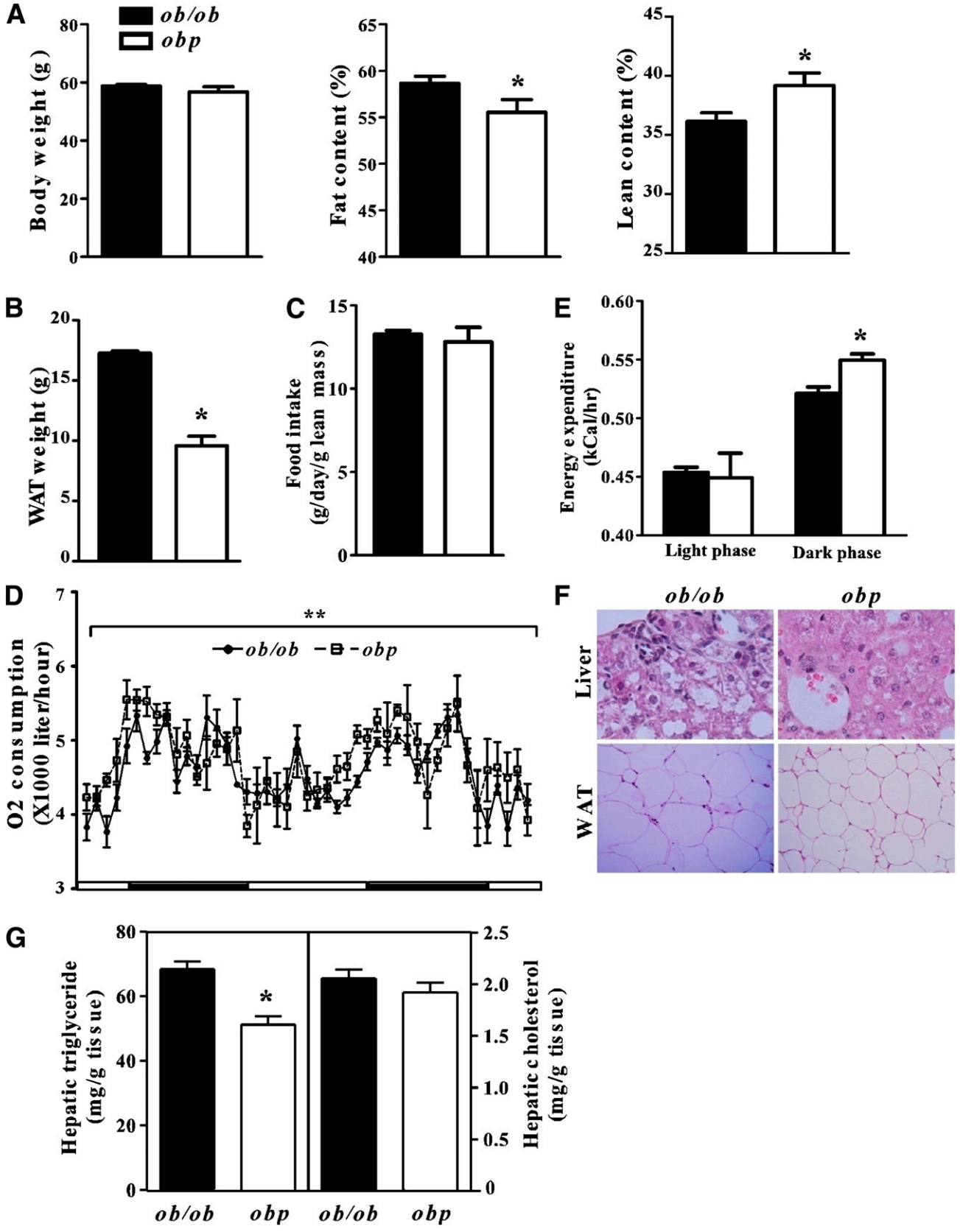

FIG. 5. PXR ablation improved metabolic function of *ob/ob* mice. *Ob/ob* and *obp* mice at 12 weeks of age were analyzed. *Obp* mice are *ob/ob* mice deficient of PXR. Body weight and body weight composition analysis (*A*), WAT weight (*B*), food intake (*C*), oxygen consumption (*D*), and energy expenditure (*E*) were measured in *ob/ob* and *obp* mice. H&E staining of the liver and WAT tissue sections (*F*) and measurement of hepatic lipid levels (*G*). $n = 4$ for each group. *$P < 0.05$, *obp* vs. *ob/ob* mice; **$P < 0.01$, *obp* vs. *ob/ob* mice. (A high-quality color representation of this figure is available in the online issue.)

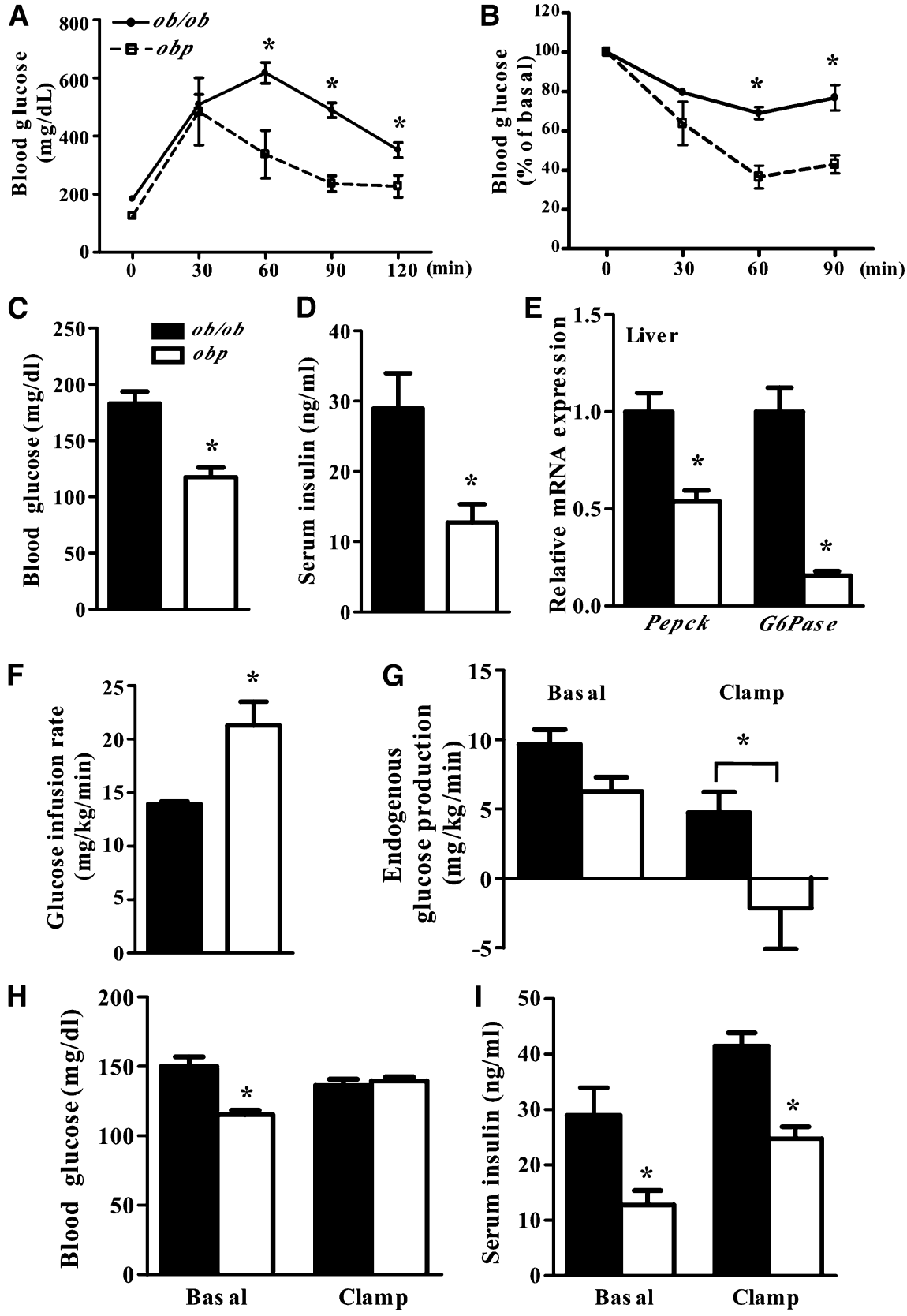

FIG. 6. PXR ablation improved insulin sensitivity in *ob/ob* mice. Mice were the same as described in Fig. 5. GTT (*A*) and ITT (*B*) tests. Blood glucose (*C*) and serum insulin (*D*) levels. *E*: The hepatic mRNA expression of gluconeogenic genes as measured by real-time PCR. Glucose infusion rate (*F*) and endogenous hepatic glucose production (*G*) during hyperinsulinemic-euglycemic clamp experiment. Blood glucose (*H*) and insulin (*I*) levels in the basal and clamp state. $n = 4$ for each group. *$P < 0.05$, *obp* vs. *ob/ob*, or the comparisons are labeled.

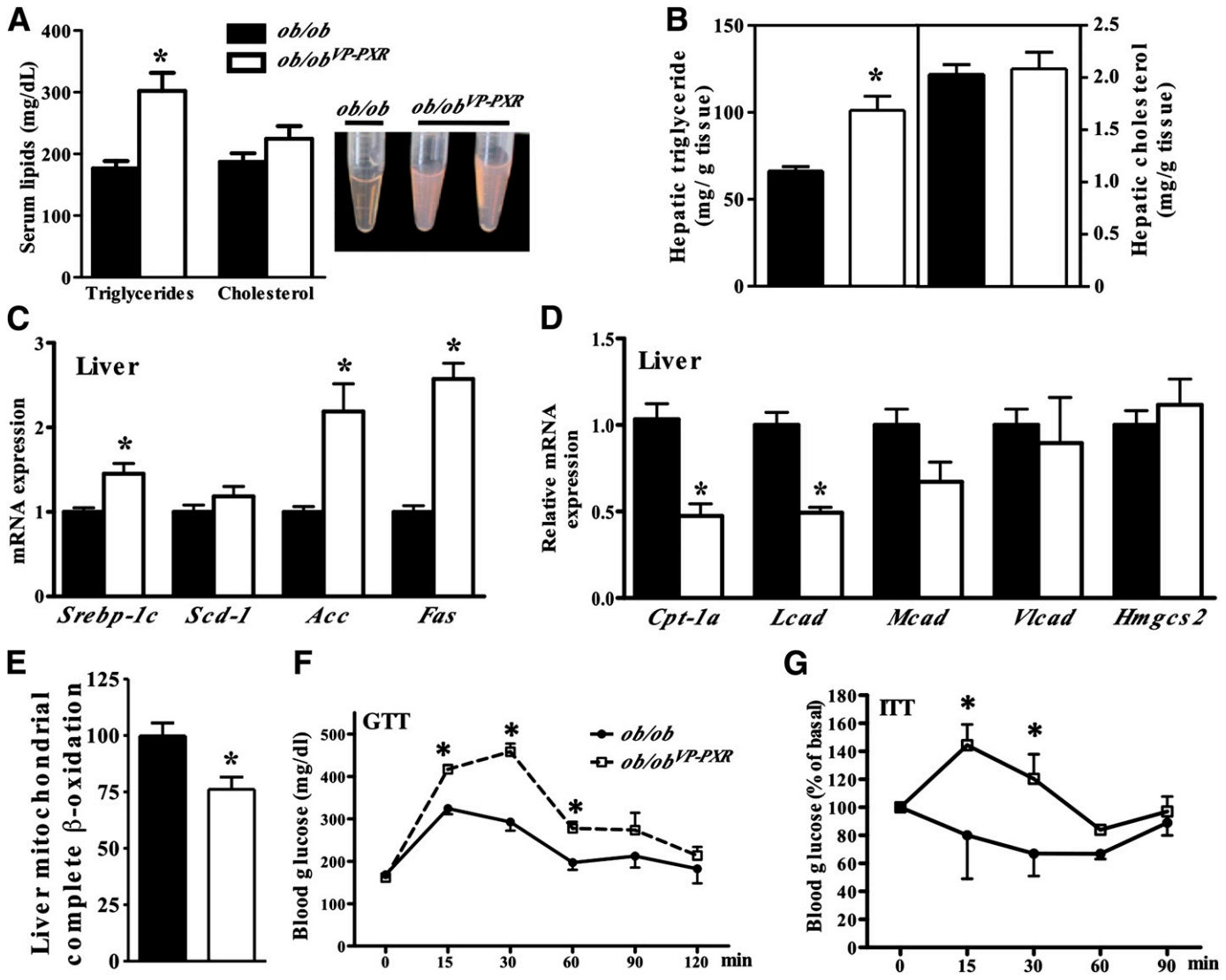

FIG. 7. PXR activation exacerbated the diabetic phenotype of *ob/ob* mice. *Ob/ob* and *ob/ob*$^{VP\text{-}PXR}$ mice at 12 weeks of age were analyzed. *Ob/ob*$^{VP\text{-}PXR}$ mice are *ob/ob* mice expressing the *Alb-VP-PXR* transgene. *A*: Measurement of serum triglyceride and cholesterol levels (*left*) and the appearance of serum (*right*). *B*: Measurement of liver triglyceride and cholesterol levels. Hepatic mRNA expression of lipogenic genes (*C*) and fatty acid oxidation genes (*D*), as measured by real-time PCR analysis. *E*: Liver fatty acid β-oxidation. GTT (*F*) and ITT (*G*). $n = 4$ for each group. *$P < 0.05$, *ob/ob* vs. *ob/ob*$^{VP\text{-}PXR}$ mice. (A high-quality color representation of this figure is available in the online issue.)

diabetic phenotype was obvious, we cannot exclude the possibility that the differences in energy expenditure, fatty acid β-oxidation, and related gene expression are secondary effects that result from body weight changes.

Recent studies showed that an elevation of fatty acid β-oxidation can reduce obesity and improve insulin resistance (34,35). We found that $PXR^{-/-}$ mice had higher energy expenditure in both the HFD and *ob/ob* models. The mitochondrial fatty acid β-oxidation was elevated and the expression of β-oxidation genes was induced in HFD-fed $PXR^{-/-}$mice, which was in contrast to the decreased β-oxidation gene expression in *ob/ob*$^{VP\text{-}PXR}$ mice. These in vivo results were consistent with a previous report that PXR binds directly to FoxA2 and represses CPT-1α gene expression. Ablation of PXR also inhibited lipogenesis, which was supported by the inhibition of lipogenic gene expression in $PXR^{-/-}$ mice. The combined effect of increased β-oxidation and decreased lipogenesis may have accounted for the inhibition of hepatic steatosis and reduced hepatic expression of proinflammatory mediators such as tumor necrosis factor-α and interleukin-6. The combined effect of lower hepatic triglyceride accumulation and inflammation might have contributed to the decreased hepatic glucose production and improved insulin sensitivity in $PXR^{-/-}$ mice. Previously, treatment of WT mice with PCN has been reported to inhibit *G6Pase* and *Pepck* gene expression (20,21). Those observations were made in chow diet–fed mice after a brief PXR ligand treatment. The discrepancies may have resulted from different nutritional and/or metabolic status, a notion that is also supported by our observation that the suppression of *G6Pase* and *Pepck* seen in chow-fed *VP-PXR* transgenic mice (19) was absent in *ob/ob*$^{VP\text{-}PXR}$ mice (data not shown).

The improved systemic insulin sensitivity in $PXR^{-/-}$ mice was supported by GTT and ITT tests, the hyperinsulinemic-euglycemic clamp, as well as ex vivo tissue analyses. Importantly, the improved insulin sensitivity was not confined to the liver, because it was also observed in the adipose tissue and skeletal muscle. Since PXR is not expressed in

the adipose tissue and skeletal muscle, the metabolic benefits of PXR ablation in the skeletal muscle and adipose tissue may have been secondary to the liver effect. In addition, we cannot exclude the metabolic effect of the loss of PXR in the intestine. Intestinal activation of PXR has recently been reported to promote hepatic steatosis (24). Mechanistically, the inhibition of JNK activation may have contributed to the amelioration of insulin resistance in $PXR^{-/-}$ mice. JNK activation has been reported to play a central role in insulin resistance (30). Cellular stresses, such as those induced by inflammation and unfolded response, can activate JNK, which in turn serine phosphorylate IRS-1 and suppress the insulin signaling pathway (31). We showed that JNK activation was reduced in HFD-fed $PXR^{-/-}$ mice, as well as in the tunicamycin-treated $PXR^{-/-}$ mouse liver. Future studies are necessary to determine the mechanism by which PXR regulates JNK activity.

The drug-induced disruption of glucose-insulin homeostasis is not uncommon in the clinic, but the mechanisms have remained elusive (5,6). PXR is a promiscuous nuclear receptor that responds to a wide variety of chemical structures. Among drugs known to induce hyperglycemia, rifampicin, statins, phenytoin, and cyclophosphamide have been shown to activate PXR. Based on our results that a sustained activation of PXR in $ob/ob^{VP\text{-}PXR}$ mice was sufficient to worsen metabolic functions, it is tempting for us to speculate that activation of PXR may represent a mechanism by which drugs induce hyperglycemia.

The effects of PXR on obesity and insulin resistance were opposite those of constitutive androstane receptor (CAR). CAR is a sister receptor of PXR that shares many functions in xenobiotic regulation. Interestingly, CAR and PXR appeared to have opposite effects on metabolic disease. We and others have reported that CAR is an antiobesity receptor that improves insulin sensitivity. Treatment of WT mice with the CAR agonist TCPOBOP inhibited both the HFD and *ob/ob* models of obesity and type 2 diabetes. In contrast, CAR ablation worsened metabolic functions (28,36). The prodiabetic effect of CAR ablation is opposite to the antidiabetic effect of PXR oblation. The antilipogenic effect of CAR activation is also opposite to the lipogenic effect of PXR activation. Although paradoxical, the current study represents an excellent example of PXR and CAR as sister receptors of overlapping, yet distinct, functions.

It was recently reported that a 7-week treatment of AKR/J mice with a high dose (50 mg/kg) of PCN prevented HFD-induced obesity and insulin resistance (25), which is not consistent with our hypothesis that activation of PXR worsens metabolic functions. There are several potential explanations for the discrepancies. First, we found that a chronic treatment with PCN is toxic to the mice. When C57BL/6J mice were treated with 20 mg/kg of PCN for 4 weeks, we found that the serum alanine aminotransferase level increased from 92 to 192 units/L, highly indicative of hepatotoxicity. Therefore, the inhibition of obesity by PCN may have been secondary to the liver toxicity, which was not thoroughly evaluated in the PCN-treated AKR/J mice (25). Secondly, their study cannot conclude that the PCN effect on obesity and insulin resistance was PXR dependent without the use of $PXR^{-/-}$ mice. Finally, mice of different genetic backgrounds were used; ours is C57BL/6J and theirs is AKR/J.

In summary, our data demonstrated that PXR ablation alleviated metabolic disorders, whereas activation of PXR exacerbated hyperlipidemia and insulin resistance. Activation of PXR may have mediated the clinic drug-responsive metabolic disorders. On the other hand, PXR antagonists may be used for the treatment of obesity and diabetes and prevention of drug-induced metabolic abnormalities. Indeed, our results showed that treatment with the PXR antagonist ketoconazole improved the metabolic function of HFD-fed mice. Unlike PXR agonists that are often associated with concerns of drug-drug interactions, PXR antagonists have been proposed as drug-sparing agents to improve the bioavailability and safety of the drugs (37). It is encouraging that major progress has been made in the development of human PXR antagonists (38–41).

ACKNOWLEDGMENTS

This work was supported in part by National Institutes of Health grants DK-083952, ES-019629 (to W.X.), DK-058855, and DK-072162 (to R.M.O.). W.X. is the Joseph Koslow Endowed Chair in Pharmaceutical Sciences at the University of Pittsburgh School of Pharmacy. J.H. was supported by an American Heart Association postdoctoral fellowship (09POST2280546). This work was also supported in part by the University of Pittsburgh Metabolic Diseases Research Center.

No potential conflicts of interest relevant to this article were reported.

J.H. designed and performed experiments and wrote the manuscript. J.G., M.X., S.R., and M.S.-R. helped with experiments. R.M.O. contributed to the discussion and review of the manuscript. W.X. obtained funding, designed experiments, and wrote the manuscript.

J.H. and W.X. are the guarantors of this work and, as such, had full access to all the data in the study and take responsibility for the integrity of the data and the accuracy of the data analysis.

The authors thank Dr. Brian N. Finck (Washington University School of Medicine, St. Louis, MO) for the lipin-1 promoter reporter gene. The authors also thank Dr. Sridhar Mani (Albert Einstein College of Medicine, New York, NY) for his advice on the in vivo regimen of ketoconazole.

REFERENCES

1. Blumberg B, Sabbagh W Jr, Juguilon H, et al. SXR, a novel steroid and xenobiotic-sensing nuclear receptor. Genes Dev 1998;12:3195–3205
2. Kliewer SA, Moore JT, Wade L, et al. An orphan nuclear receptor activated by pregnanes defines a novel steroid signaling pathway. Cell 1998;92:73–82
3. Ihunnah CA, Jiang M, Xie W. Nuclear receptor PXR, transcriptional circuits and metabolic relevance. Biochim Biophys Acta 2011;1812:956–963
4. Cheng J, Shah YM, Gonzalez FJ. Pregnane X receptor as a target for treatment of inflammatory bowel disorders. Trends Pharmacol Sci 2012;33:323–330
5. Luna B, Feinglos MN. Drug-induced hyperglycemia. JAMA 2001;286:1945–1948
6. Pandit MK, Burke J, Gustafson AB, Minocha A, Peiris AN. Drug-induced disorders of glucose tolerance. Ann Intern Med 1993;118:529–539
7. Howe K, Sanat F, Thumser AE, Coleman T, Plant N. The statin class of HMG-CoA reductase inhibitors demonstrate differential activation of the nuclear receptors PXR, CAR and FXR, as well as their downstream target genes. Xenobiotica 2011;41:519–529
8. Luo G, Cunningham M, Kim S, et al. CYP3A4 induction by drugs: correlation between a pregnane X receptor reporter gene assay and CYP3A4 expression in human hepatocytes. Drug Metab Dispos 2002;30:795–804
9. Lindley C, Hamilton G, McCune JS, et al. The effect of cyclophosphamide with and without dexamethasone on cytochrome P450 3A4 and 2B6 in human hepatocytes. Drug Metab Dispos 2002;30:814–822
10. Takasu N, Yamada T, Miura H, et al. Rifampicin-induced early phase hyperglycemia in humans. Am Rev Respir Dis 1982;125:23–27
11. Preiss D, Sattar N. Statins and the risk of new-onset diabetes: a review of recent evidence. Curr Opin Lipidol 2011;22:460–466

12. al-Rubeaan K, Ryan EA. Phenytoin-induced insulin insensitivity. Diabet Med 1991;8:968–970
13. Banner W Jr, Johnson DG, Walson PD, Jung D. Effects of single large doses of phenytoin on glucose homeostasis—a preliminary report. J Clin Pharmacol 1982;22:79–81
14. Carter BL, Small RE, Mandel MD, Starkman MT. Phenytoin-induced hyperglycemia. Am J Hosp Pharm 1981;38:1508–1512
15. Peters BH, Samaan NA. Hyperglycemia with relative hypoinsulinemia in diphenylhydantoin toxicity. N Engl J Med 1969;281:91–92
16. Suvannasankha A, Fausel C, Juliar BE, et al. Final report of toxicity and efficacy of a phase II study of oral cyclophosphamide, thalidomide, and prednisone for patients with relapsed or refractory multiple myeloma: a Hoosier Oncology Group Trial, HEM01-21. Oncologist 2007;12:99–106
17. Weiser MA, Cabanillas ME, Konopleva M, et al. Relation between the duration of remission and hyperglycemia during induction chemotherapy for acute lymphocytic leukemia with a hyperfractionated cyclophosphamide, vincristine, doxorubicin, and dexamethasone/methotrexate-cytarabine regimen. Cancer 2004;100:1179–1185
18. Nakamura K, Moore R, Negishi M, Sueyoshi T. Nuclear pregnane X receptor cross-talk with FoxA2 to mediate drug-induced regulation of lipid metabolism in fasting mouse liver. J Biol Chem 2007;282:9768–9776
19. Zhou J, Zhai Y, Mu Y, et al. A novel pregnane X receptor-mediated and sterol regulatory element-binding protein-independent lipogenic pathway. J Biol Chem 2006;281:15013–15020
20. Kodama S, Koike C, Negishi M, Yamamoto Y. Nuclear receptors CAR and PXR cross talk with FOXO1 to regulate genes that encode drug-metabolizing and gluconeogenic enzymes. Mol Cell Biol 2004;24:7931–7940
21. Kodama S, Moore R, Yamamoto Y, Negishi M. Human nuclear pregnane X receptor cross-talk with CREB to repress cAMP activation of the glucose-6-phosphatase gene. Biochem J 2007;407:373–381
22. Bhalla S, Ozalp C, Fang S, Xiang L, Kemper JK. Ligand-activated pregnane X receptor interferes with HNF-4 signaling by targeting a common coactivator PGC-1alpha. Functional implications in hepatic cholesterol and glucose metabolism. J Biol Chem 2004;279:45139–45147
23. Gao J, Xie W. Pregnane X receptor and constitutive androstane receptor at the crossroads of drug metabolism and energy metabolism. Drug Metab Dispos 2010;38:2091–2095
24. Cheng J, Krausz KW, Tanaka N, Gonzalez FJ. Chronic exposure to rifaximin causes hepatic steatosis in pregnane X receptor-humanized mice. Toxicol Sci 2012;129:456–468
25. Ma Y, Liu D. Activation of pregnane X receptor by pregnenolone 16 α-carbonitrile prevents high-fat diet-induced obesity in AKR/J mice. PLoS ONE 2012;7:e38734
26. Xie W, Barwick JL, Downes M, et al. Humanized xenobiotic response in mice expressing nuclear receptor SXR. Nature 2000;406:435–439
27. Gao J, He J, Shi X, et al. Sex-specific effect of estrogen sulfotransferase on mouse models of type 2 diabetes. Diabetes 2012;61:1543–1551
28. Gao J, He J, Zhai Y, Wada T, Xie W. The constitutive androstane receptor is an anti-obesity nuclear receptor that improves insulin sensitivity. J Biol Chem 2009;284:25984–25992
29. Chen HC, Farese RV Jr. Determination of adipocyte size by computer image analysis. J Lipid Res 2002;43:986–989
30. Hirosumi J, Tuncman G, Chang L, et al. A central role for JNK in obesity and insulin resistance. Nature 2002;420:333–336
31. Vallerie SN, Hotamisligil GS. The role of JNK proteins in metabolism. Sci Transl Med 2010;2:rv5
32. Bou Khalil M, Sundaram M, Zhang HY, et al. The level and compartmentalization of phosphatidate phosphatase-1 (lipin-1) control the assembly and secretion of hepatic VLDL. J Lipid Res 2009;50:47–58
33. Ryu D, Oh KJ, Jo HY, et al. TORC2 regulates hepatic insulin signaling via a mammalian phosphatidic acid phosphatase, LIPIN1. Cell Metab 2009;9:240–251
34. Huang J, Jia Y, Fu T, et al. Sustained activation of CptR{alpha} by endogenous ligands increases hepatic fatty acid oxidation and prevents obesity in ob/ob mice. FASEB J 2012;26:628–638
35. Orellana-Gavaldà JM, Herrero L, Malandrino MI, et al. Molecular therapy for obesity and diabetes based on a long-term increase in hepatic fatty-acid oxidation. Hepatology 2011;53:821–832
36. Dong B, Saha PK, Huang W, et al. Activation of nuclear receptor CAR ameliorates diabetes and fatty liver disease. Proc Natl Acad Sci USA 2009;106:18831–18836
37. Venkatesh M, Wang H, Cayer J, et al. In vivo and in vitro characterization of a first-in-class novel azole analog that targets pregnane X receptor activation. Mol Pharmacol 2011;80:124–135
38. Das BC, Madhukumar AV, Anguiano J, et al. Synthesis of novel ketoconazole derivatives as inhibitors of the human pregnane X receptor (PXR; NR1I2; also termed SXR, PAR). Bioorg Med Chem Lett 2008;18:3974–3977
39. Ekins S, Kholodovych V, Ai N, et al. Computational discovery of novel low micromolar human pregnane X receptor antagonists. Mol Pharmacol 2008;74:662–672
40. Huang H, Wang H, Sinz M, et al. Inhibition of drug metabolism by blocking the activation of nuclear receptors by ketoconazole. Oncogene 2007;26:258–268
41. Wang H, Li H, Moore LB, et al. The phytoestrogen coumestrol is a naturally occurring antagonist of the human pregnane X receptor. Mol Endocrinol 2008;22:838–857